International Journal of Fatigue 33 (2011) 1205–1220

Contents lists available at ScienceDirect

International Journal of Fatigue

journal homepage: www.elsevier.com/locate/ijfatigue

The role of strain ratcheting and mesh refinement in finite element analyses of plasticity induced crack closure

Kristine B. Cochran [a], Robert H. Dodds [b,*], Keith D. Hjelmstad [c]

[a] Oak Ridge National Laboratory, Oak Ridge, TN 37831, USA
[b] Department of Civil & Environmental Engineering, University of Illinois,Urbana, IL 61801, USA
[c] Arizona State University, Mesa, AZ 85212, USA

ARTICLE INFO

Article history:
Received 16 June 2010
Received in revised form 3 March 2011
Accepted 11 March 2011
Available online 17 March 2011

Keywords:
Crack closure
Small-scale yielding
Finite element analysis
Mesh dependence
Cycle dependence
Nonlinear plasticity

ABSTRACT

Numerical investigations of plasticity induced crack closure using the finite element method typically assume: (1) the opening behavior remains independent of the simulated rate of crack growth, and (2) a threshold element size exists below which crack opening loads become mesh independent. Nevertheless, examples in the recent literature and also in the present work indicate these assumptions do not always hold. The current work demonstrates the field results (displacements, stress–strain) for cyclic loading of stationary cracks converge with mesh refinement. However, when the cyclic load regime includes systematic crack extension, certain conditions lead to highly mesh dependent fields and opening loads. The cyclic accumulation of permanent deformation (strain ratcheting) *necessarily* produces mesh dependence when the finite element size dictates the rate of crack growth. Moreover, extensive ratcheting leads to physically unrealistic shapes of the crack opening profiles. This work explores the link between strain ratcheting, mesh dependence and load-cycle effects within a small-scale yielding framework, including the influence of plane strain *vs.* plane stress constraints, constitutive definition (non-hardening, linear kinematic hardening and nonlinear kinematic hardening) and the monotonic flow properties. Key conclusions from this work include: (1) near-tip strain ratcheting generally increases with decreased hardening and can be much more pronounced in plane strain than in plane stress; (2) for models with significant ratcheting, slower rates of simulated growth due to smaller element size and/or more load cycles between crack advancements generally reduce the opening loads; and (3) the computed opening loads depend intrinsically on the amount of ratcheting, and the rate of crack growth as determined by the element size and number of load cycles between crack advancements.

1. Introduction

Beginning with Elber's [1] recognition of the phenomenon in 1970, plasticity induced crack closure (PICC) has remained an active area of research both experimentally and numerically. Crack closure, the premature contact of crack faces on unloading and delayed opening with reloading, may reduce significantly the observed crack-growth rate relative to that expected from the range of applied loading alone. Crack closure arises from various sources including surface roughness and oxide formation, but inelastic deformation generally forms the dominant mechanism for moderate-to-high applied stress levels and crack lengths at engineering scales. PICC stems from the accumulation of residual plastic deformation on the crack faces. The severe stress concentration ahead of the advancing crack tip produces a zone of plastically yielded material. As the crack grows through this plastic zone, the permanent deformation becomes part of the crack wake. The crack faces close earlier on unloading, creating a region of compressive residual stresses, and open later on reloading, once the increased loads overcome the residual stresses.

For mode I small-scale yielding, the stress-intensity factor (K_I) sets the amplitude of the fields (displacement, stress–strain) in the linear-elastic material enclosing the crack-tip plastic zone. K_I reflects the magnitude and configuration of the applied load, the crack size and location, and the geometry of the component/specimen. Experimental results confirm the change in an effective stress intensity factor, $\Delta K_{eff} = K_{max} - K_{op}$, drives the crack-growth rate in each cyle, where K_{max} denotes the maximum applied load (K_I) and K_{op} indicates the load at which the crack faces become fully open [1]. This model implies the accumulation of fatigue damage only when the crack remains fully open. PICC thus retards the rate of crack growth by reducing the crack-open portion of a load cycle.

Quantifying the values of K_{op} under wide-ranging conditions remains the subject of numerous experimental and numerical

* Corresponding author.
E-mail addresses: cochrankb@ornl.gov (K.B. Cochran), rdodds@illinois.edu (R.H. Dodds), Keith.Hjelmstad@asu.edu (K.D. Hjelmstad).

0142-1123/$ - see front matter © 2011 Elsevier Ltd. All rights reserved.
doi:10.1016/j.ijfatigue.2011.03.005

studies. The gradual nature of the crack opening/closing process and the many geometry-material-loading conditions encountered in practice make finite element analyses attractive to estimate K_{op} levels for engineering applications. Nevertheless, the complex features of fatigue crack growth together with the numerical difficulties of such highly nonlinear response lead to significant modeling challenges – including mesh sensitivity, crack-growth algorithms, opening-detection procedures, contact, and the realistic simulation of cyclic plastic deformation.

This study began as a seemingly straightforward extension to the substantial body of PICC modeling work. Most PICC models employ a standard protocol for developing a mesh, growing the crack, and quantifying closure/opening load levels. The literature displays some variations of the protocol initiated by Newman [2] in 1976 but the fundamental aspects persist today. Working within this framework, Roychowdhury and Dodds [3,4] developed a 3D small-scale yielding (SSY) model to analyze PICC in thin plates using simple, kinematic hardening with a constant plastic modulus. To extend the 3D SSY model, the next (seemingly straightforward) task focused on PICC with more realistic material behavior, *e.g.*, nonlinear kinematic hardening.

Initial 3D SSY analyses revealed crack-front opening loads strongly dependent on the element size for nonlinear plasticity models – Armstrong and Frederick's nonlinear kinematic hardening model [5] and Lubliner's Generalized Plasticity model [6]. Mesh independent fields and opening loads became quite elusive, to the point that numerical issues obscured any insight into the physical behavior. Thus, the investigation turned to studying how and why finite element models for plasticity induced crack closure exhibit such (often pronounced) sensitivity to the element size.

The present study examines mesh refinement and cyclic loading effects on displacements, stress–strain fields, and opening loads in 2D SSY finite element models of both stationary and growing cracks. The boundary layer model of a mode I crack features constant amplitude, $R = 0$, and zero T-stress loading applied to the remote boundary. All analyses employ the ABAQUS [7] software and its built-in elastic–plastic constitutive models, which include linear kinematic hardening and cyclic plasticity (nonlinear kinematic hardening).

For stationary cracks, the opening profiles and stress–strain fields ahead of the crack tip converge with mesh refinement for both linear and nonlinear hardening material models under plane-stress and plane-strain conditions. The nonlinear hardening model produces changes in cyclic displacements and stresses due to the strain ratcheting and stress relaxation inherent in the constitutive formulation for both plane-stress and plane-strain conditions. However, under plane-strain conditions an elastic–perfectly plastic material and materials modeled with linear (kinematic) hardening having a low plastic modulus exhibit strain ratcheting which can be extensive and very slow to saturate with an increased number of constant amplitude load cycles (not a function of mesh refinement).

With periodic crack growth enforced by user-controlled node release, these cyclic changes in stresses and strains lead to mesh dependent opening profiles, stress–strain fields, and opening loads. In this very commonly employed method to model crack advance, the crack grows in length by one element size every specified number of load cycles. Thus the parameters that govern crack-growth rate become the element size coupled with the number of load cycles between node releases. A reduction of the element size without changing the number of load cycles between crack advances requires more load cycles to achieve the same amount of crack growth. Similarly, an increase in the number of load cycles between crack advancements for a constant element size reduces the rate of crack growth and increases the total number of load cycles. For constitutive models and load paths that generate ratcheting behavior, the link between crack-growth rate and cyclic loading history renders the fields and opening loads necessarily dependent on the crack-growth parameters. These effects of computational crack-growth rate and strain ratcheting on opening loads have implications discussed here for the interpretation of some past PICC finite element results and the planning of future studies.

The outline for this paper is as follows. Section 2 reviews prior numerical studies reporting mesh dependence or the influence of load cycles in PICC models. Section 3 describes details of the models employed in the current study. Section 4 presents and discusses key results from the current analyses. Section 5 summarizes the major findings and develops the main conclusions of this work. The appendix develops simple solutions to illustrate the ratcheting behavior of elastic–perfectly plastic and linear (kinematic) hardening material models under non-proportional loading paths including uniaxial, plane-strain loading.

2. Background

This section presents a brief review of the work most relevant to the current investigation on mesh refinement and crack growth issues. For more complete overviews of PICC finite element modeling, refer to the works of McClung [8] and Solanki et al. [9]. For a more detailed discourse on mesh refinement issues in the literature see [10].

The work of McClung and Sehitoglu [11] continues to influence a large portion of PICC finite element studies with respect to element refinement. Stemming from the work of Newman [2], McClung and Sehitoglu suggest at least 10, bilinear quadrilateral elements are needed in the forward plastic zone for 2D analyses. McClung and Sehitoglu present caveats to their recommendation (including the potential role of the reverse plastic zone and the unknown behavior with further mesh refinement). Further, their work focused on material behavior modeled with linear kinematic hardening and plane stress conditions, conditions for which agreement between numerical and some experimental studies exist, *e.g.* [2,12,13]. Nevertheless, many subsequent studies treat the 10 element rule as universal and forgo case-specific mesh refinement studies. Unfortunately, significant evidence contradicting the 10 element rule now exists.

Gonzalez-Herrera and Zapatero [14] reveal mesh size effects that do not conform with the 10 element rule in their investigation of a C(T) specimen with linear hardening materials in both plane-stress and plane-strain conditions. Increased mesh refinement beyond 10 elements in the forward plastic zone first increases opening loads until a maximum level is reached after which still further refinement decreases opening loads. They show that the R-ratio influences the degree of mesh dependence. For linear hardening in plane stress with $R = 0.3$, opening loads appear converged for element sizes on the order of 1% of the initial plastic zone. No convergence occurs for $R = 0.1$ loading. They report similar mesh refinement effects in plane strain and advocate linear extrapolation of the decreasing opening loads to a zero mesh size. In their studies of an M(T) specimen in plane stress with large strain kinematics, linear plasticity, and quadratic elements, Antunes et al. [15] find the element size and the rate of crack growth can influence opening loads significantly. With isotropic hardening, mesh refinement continues to produce more closure (higher opening loads). With kinematic hardening, opening loads increase with initial element size reduction but after reaching a maximum level, further refinement reduces opening loads. They vary the element size while holding the instantaneous amount of crack growth constant by growing the crack multiple elements at a time showing that the incremental crack growth amount is a factor in mesh dependence.

Additionally, they demonstrate the number of load cycles between crack advancement has a larger effect on opening loads for finer meshes than for coarser meshes.

Solanki et al. [16] investigate element size effects with an elastic–perfectly plastic material model for both C(T) and M(T) specimens in plane stress and plane strain. For both specimen types in plane stress, and for the M(T) specimen in plane strain, the opening loads appear to converge with mesh refinement. For the plane stress cases, convergence develops with an element size on the order of 10% of the forward plastic zone. For the M(T) specimen in plane strain, convergence occurs when the element size is approximately 4% of the forward plastic zone. The C(T) specimen in plane strain produces mesh dependent opening loads for all meshes in the study. The authors suggest this may indicate closure does not actually occur for this specimen in a plane strain model and discourage extrapolation of the opening loads to zero element size. They attribute the lack of closure to the tensile T-stress of the C(T) specimen which resists plastic flow.

Jiang et al. [17] analyze an M(T) specimen under plane-stress conditions with large-strain kinematics and find convergence depends strongly on the material model. For elastic–perfectly plastic material behavior, they demonstrate the opening load continues to decrease with decreasing mesh size. A similar, though less pronounced, trend occurs with linear kinematic hardening. Using a cyclic material model developed by Jiang and Sehitoglu [18,19], they report opening loads to be reasonably mesh independent over an element-size range from approximately 40% to 4% of the estimated cyclic plastic zone size. However, they observe a decrease in opening load with further decrease in element size and do not carry the mesh refinement to the extent for this material model as for the elastic–perfectly plastic and linear kinematic hardening models. Jiang et al. also repeat the work of Solanki et al. [16] for the M(T) plane stress case (a "converging" case, see above) but find further mesh refinement leads to mesh dependent opening loads. Noting the computational effort to grow the crack sufficiently to achieve stabilized opening loads for a highly refined mesh, Jiang et al. recommend extrapolation of the opening load with amount of crack growth using an exponential relationship.

The number of load cycles between crack-growth increments couples with the mesh refinement issues. The use of more than one load cycle between crack advancements is a common technique described in the literature. Many researchers apply two load cycles between crack advancements and compute opening loads during the second cycle after advancement, *e.g.*, [20–23] and a few consider more than two load cycles [24,25].

The work by de Matos and Nowell [24] describes some novel and important observations about the effects of load cycling between node releases. For an elastic–perfectly plastic material in plane stress, opening loads differ if the applied load regime uses one or two cycles between crack growth, but higher numbers of cycles do not change the results further. For plane strain and 3D models, the opening behavior does not stabilize with increasing load cycles between crack advancements as quickly, if at all.

Antunes and Rodrigues [21] examine the effect of load cycling between crack advancements using a nonlinear hardening material model in plane stress. They report that, in general, two cycles are sufficient to stabilize the plastic deformation and thus the opening loads. Nevertheless, they show the opening displacement of the first node behind the crack tip continues to increase with repetitive load cycling during suspended crack advance.

Jiang et al. [17] find additional load cycles between crack-growth increments decrease opening loads significantly. They examine the effect of 190 cycles but note most of the change in opening load occurs over the first four cycles. In their plane-strain studies with the Chaboche model, Zhao et al. [25] demonstrate the stress and strain fields continue to undergo significant changes even after fifty load cycles on a stationary crack but nonetheless proceed with two load cycles per crack advancement for their studies with a growing crack.

In their plane-strain, crack-closure analyses with the Chaboche model, Pommier and Bompard [23] determine that the "hysteresis loop at the crack tip stabilizes at the second cycle". Nevertheless, for calibrations that use only isotropic hardening, Pommier [26] finds using six cycles (instead of two) between node releases lowers the opening loads for all examined conditions. Pommier comments there should be a relationship between the rate of strain hardening and the simulated rate of crack growth.

In the second part of their extensive study on PICC analysis, McClung and Sehitoglu [27] discuss a link between rate of crack growth and cyclic material behavior, in terms of cyclic mean stress relaxation. They note that more load cycles per crack advance decreases opening loads for a power-law hardening material model that undergoes cyclic stress relaxation and strain ratcheting. The present paper explores the issues of numerical crack-growth rate and cyclic material response as they correlate to mesh refinement effects on opening loads.

3. Numerical procedures

3.1. Small-scale yielding framework

This work considers a subset of fatigue crack growth problems characterized by initially sharp, through cracks in metallic components subject to constant amplitude, mode I loading. Small-scale yielding (SSY) conditions follow from the maximum level of the applied remote load which limits plasticity to a small zone around the crack tip, with the remainder of the model remaining linear-elastic. Under SSY conditions, the plastic zone size (r_p), as measured along the crack plane ahead of the crack tip, becomes proportional to $(K_I/\sigma_y)^2$, where σ_y denotes the yield stress. In a 3D setting, K_I, σ_y, and the thickness (B) form the basis of a powerful similiarity scaling relationship developed by Roychowdhury and Dodds [3,4,28]. Displacements, stress–strain fields and opening behavior exhibit strong thickness variation in the 3D SSY simulations. Nevertheless, this work examines 2D SSY models, in the interest of clearly demonstrating and explaining the root cause of mesh refinement and crack growth issues.

In a SSY boundary-layer model, the displacement and stress–strain fields outside of the plastic zone follow those of the linear-elastic, mode I loading for either plane stress or plane strain conditions. At a radius $\overline{R}$ from the crack tip, such that $\overline{R} \gg r_p$, the displacement fields for the mode I, linear-elastic conditions are

$$\begin{aligned} u_x &= \frac{K_I}{2G}\sqrt{\frac{\overline{R}}{2\pi}}\cos\left(\frac{\theta}{2}\right)\left[\kappa - 1 + 2\sin^2\left(\frac{\theta}{2}\right)\right] \\ u_y &= \frac{K_I}{2G}\sqrt{\frac{\overline{R}}{2\pi}}\sin\left(\frac{\theta}{2}\right)\left[\kappa + 1 - 2\cos^2\left(\frac{\theta}{2}\right)\right] \end{aligned} \tag{1}$$

where u_x is the displacement parallel to the crack plane, u_y is the displacement perpendicular to the crack plane, $\kappa = (3 - \nu)/(1 + \nu)$ for plane stress and $\kappa = 3 - 4\nu$ for plane strain, ν is Poisson's ratio, G is the shear modulus, and K_I is the mode I stress-intensity factor. These equations do not include T-stress effects, *i.e.*, $T = 0$ in all present analyses.

3.2. Mesh

The boundary-layer approach generalizes a large number of practical SSY applications, reducing the need for specimen specific meshes. Symmetry about the crack surface allows modeling only half the cylindrical domain containing an edge crack terminating near the center of the cylinder, refer to Fig. 1a. Displacement

boundary conditions along the crack ligament and contact algorithms along the crack face enforce the symmetry.

Fig. 1b and c show typical mesh details of the relevant region in 2D, mode I loading. A band of small, uniform elements around the crack tip of length and height L_e provide field resolution and crack growth. The small-strain, 4-node elements employ either a plane-stress or plane-strain formulation, as noted. The various meshes constructed for the analyses provide a range of approximately 10–400 elements in the forward plastic zone. The finest mesh has 10,243 nodes and 9793 elements.

3.3. Material models

This study employs plasticity models available in ABAQUS including non-hardening (elastic–perfect plasticity), linear kinematic hardening, and nonlinear kinematic hardening (known as the Chaboche model or Armstrong & Frederick's model). The models have several features in common – all are rate-independent, continuum-based, elastoplastic models. They use additive decomposition of the strain into elastic and plastic components. The von Mises yield surface defines the elastic domain;

$$f(\boldsymbol{s},\boldsymbol{\alpha}) = \|\boldsymbol{s}-\boldsymbol{\alpha}\| - \sqrt{\frac{2}{3}}\sigma_y \tag{2}$$

where $\boldsymbol{s}$ is the deviatoric stress tensor ($\boldsymbol{s} = \sigma - \frac{1}{3}tr(\boldsymbol{\sigma})\boldsymbol{I}$), $\boldsymbol{\alpha}$ is the backstress tensor, and $\|\ ()\ \|$ indicates the 2-norm.

Plastic yielding occurs via an associative flow rule as

$$\dot{\boldsymbol{\epsilon}}^p = \dot{\lambda}\frac{df}{d\boldsymbol{\sigma}} \tag{3}$$

such that $\dot{\boldsymbol{\epsilon}}^p$ is the rate of plastic strain and $\dot{\lambda}$ is a consistency parameter to constrain plastic states to the yield surface.

Eq. 4 describes the nonlinear hardening rule governing backstress evolution, where C and γ are material parameters, $\boldsymbol{n}$ is the normal to the yield surface, and $\dot{\boldsymbol{\alpha}} = \sqrt{\frac{2}{3}\dot{\boldsymbol{\epsilon}}^p : \dot{\boldsymbol{\epsilon}}^p}$ is the equivalent plastic strain rate.

$$\dot{\boldsymbol{\alpha}} = \dot{\bar{\epsilon}}^p(C\boldsymbol{n} - \gamma\boldsymbol{\alpha}) \tag{4}$$

Setting $\gamma = 0$ recovers linear kinematic hardening while setting both γ and C to 0 establishes elastic–perfect plasticity.

In uniaxial monotonic loading, the linear kinematic hardening manifests as a bilinear stress–strain response; an initial elastic response with slope E abruptly changes to slope E_T at the yield point, σ_y. Here E_T describes the constant tangent after initial yielding while C sets the slope of the stress–plastic strain response; $C = EE_T/(E - E_T)$. Linear kinematic hardening is referred to here as linear hardening. The elastic–perfectly plastic model is simply the linear hardening model with $E_T = 0$. The nonlinear kinematic hardening model has a distinct yield point but, in monotonic loading, the post-yield slope decreases with increasing plastic strain to asymptotically perfectly plastic behavior. See Fig. 2a for representative uniaxial monotonic behavior.

Fig. 2b and c demonstrates the uniaxial cyclic response of the three material models. Fig. 2c does not show the the elastic–perfectly plastic model because it does not accommodate uniaxial stress-controlled loading beyond the linear-elastic region. In uniaxial non-symmetric loading, the nonlinear model can produce both stress relaxation Fig. 2b) and strain ratcheting Fig. 2c. The linear kinematic hardening and elastic–perfectly plastic models do not exhibit either relaxation or ratcheting in uniaxial, plane-stress loading. Nevertheless, under certain types of loading these models will produce these cyclic effects. The results sections and appendix discuss this issue in more detail. See [6,7,10] for further information on these three material models.

For all material models in this study, $E = 185$ GPa and $\nu = 0.3$. For the linear hardening model $\sigma_y = 1.08$ GPa and $E_T = 0.2E$ unless otherwise indicated. The nonlinear hardening model uses $\sigma_y = 0.674$ GPa, $C = 413$ GPa and $\gamma = 735$, following the definitions of the material parameters in the ABAQUS manual [7].

3.4. Loading, boundary conditions, and opening detection

Cyclically varying displacement boundary conditions on the outer circumference of the mesh impose the remote loading. The stress intensity factor, K_I, controls the magnitude of the displacements (u_x and u_y) through the linear-elastic plane-stress or plane-strain fields defined above. A typical load cycle ramps K_I from 0 to K_{max} and then back to zero ($R = 0$ loading). The load increments are relatively fine at the beginning and end of each cycle to capture the crack opening and closing behavior. At maximum load, the

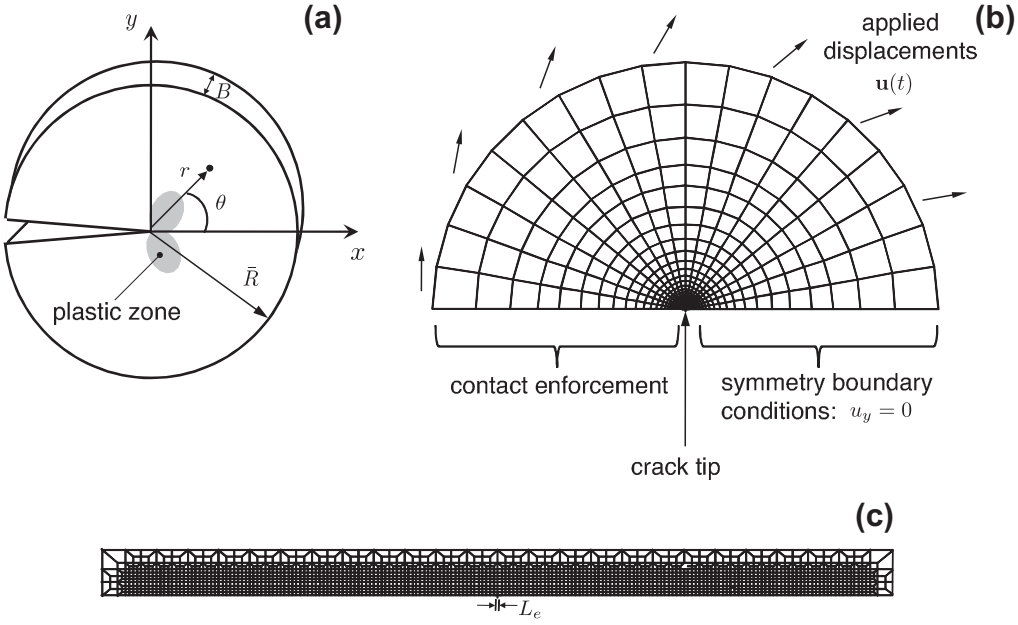

Fig. 1. Small-scale yielding boundary layer model and typical finite element mesh: (a) boundary layer domain with small crack-tip plastic zone enclosed by linear-elastic region; (b) typical 2D mesh, full view; and (c) near crack-tip region comprised of small, uniform elements.

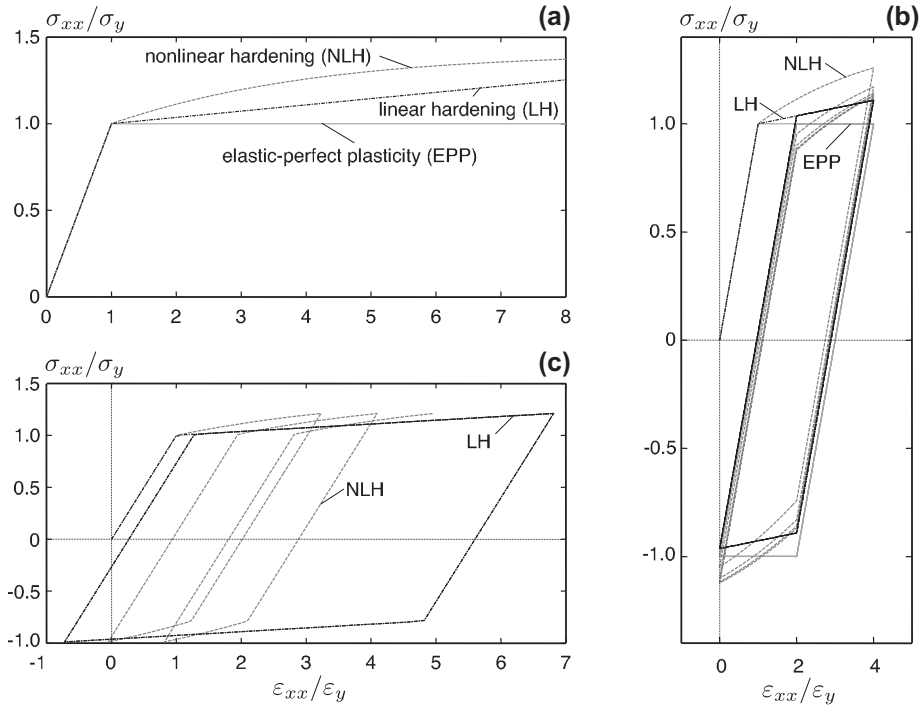

Fig. 2. Material model response under uniaxial loading: (a) monotonic loading; (b) nonsymmetric strain-controlled cyclic loading; and (c) nonsymmetric stress-controlled cyclic loading.

crack typically grows by one element per cycle such that the amount of crack growth per cycle, δa, is equal to L_e. A 5-increments redistribution scheme (internal to ABAQUS) eliminates the reactions at the previous crack-tip node. K_I is held constant during the redistribution increments to facilitate convergence of the Newton iterations at each increment. A typical cycle has 65 load increments. ABAQUS's default tolerance to terminate Newton iterations proves insufficient for the finer meshes; these analyses instead use a tolerance of 10^{-5} on the ratio of maximum residual to average force (default tolerance is 0.005). For the current study, K_{max} is $32\text{MPa}\sqrt{\text{m}}$ and the forward plastic zone size is on the order of 0.5 mm for plane stress (with thickness $B = 1.0$ mm) .

Upon the loss of symmetry-plane contact of the node(s) behind the crack tip, the current value of the applied K_I becomes the opening "load", K_{op}. This work examines the opening load evolution with crack growth at the second node behind the crack tip, as well as the opening load variation with physical distance from the current tip during one load cycle. The resolution of the opening detection depends on the increment size; a node closed at increment i of a cycle may be open at increment $i + 1$.

4. Results and discussion

This section presents numerical results to examine element size and cyclic loading effects on crack-tip opening loads, opening profiles, and stress–strain fields. Supporting analyses employ the 2D boundary-layer model with small-scale yielding (SSY), mode I conditions. The outline for this section is as follows.

1. Numerical results illustrate the non-convergence of crack opening loads with element mesh refinement and the choice of material constitutive formulation in the simplest form: crack extension in plane stress with linear kinematic hardening *vs.* nonlinear kinematic hardening.
2. Solutions of the SSY model without crack growth for both monotonic and cyclic loads clarify the roles of element refinement and constitutive models on opening profiles and stress–strain fields.
3. Introduction of crack growth via programmed node release demonstrates that cyclic changes in material response (*e.g.*, ratcheting) form the root cause of the commonly observed element size dependence.
4. Cyclic effects occur with the simple linear hardening model and elastic–perfect plasticity in plane strain, leading again to a strong mesh dependence of crack opening loads.
5. Analyses investigate the impact of the number of specified load cycles between node releases on opening profiles and plastic strain histories for solutions with both non-hardening and linear hardening material models.
6. The last section re-examines element size dependence of crack opening loads in nonlinear hardening analyses with cyclic loading effects minimized via an imposed mesh-independent effective growth rate, *i.e.*, balancing mesh refinement with the specified number of cycles to achieve the same computational, crack-growth rates and thus similar crack opening loads.

4.1. Mesh dependence of opening loads

As shown in the work of Roychowdhury and Dodds [3], 3D analyses with the linear kinematic hardening model achieve opening loads relatively insensitive to mesh refinement, provided the element size is small enough to resolve adequately both the forward and reverse plastic zones. With only the material constitutive behavior changed to nonlinear kinematic hardening, the same finite element models produce non-convergent opening loads even for highly refined meshes. Fig. 3 highlights the element size effects with linear and nonlinear kinematic hardening material models. Although the trends are similar in 3D, this figure and discussion

eliminates through-thickness complexities by considering simpler plane-stress analyses. The graphs show the evolution in normalized opening load (based on the second node behind the current crack tip) as the crack grows up to twice the size of the initial, forward plastic zone $\left(\Delta a/r_p^{for}=2\right)$ that develops at peak load on the first load cycle before crack growth. Here, Δa defines the total amount of crack growth and r_p^{for} denotes the size of the plastic zone along the uncracked ligament ahead of the crack tip at peak load. The measure of relative element size, r_p^{for}/L_e, indicates the number of elements residing in the initial forward plastic zone. For these analyses, the crack advances by one element length at the peak of each load cycle.

For the linear hardening model (Fig. 3a), opening loads for the three coarsest meshes are nearly identical and are indistinguishable at steady-state. Opening loads from the finest mesh lie slightly above the other three meshes, but within the resolution of the opening detection procedure of the contact formulation. The value of the opening load changes for different plastic moduli (generally higher opening loads for smaller plastic moduli) but remains mesh independent. For the nonlinear hardening model (Fig. 3b), the evolution of opening loads displays pronounced mesh dependencies. With initial refinement (the coarsest three meshes), opening loads increase with decreasing mesh size. Although intermediate mesh sizes produce similar opening loads at steady state, continued mesh refinement lowers the opening loads. This trend typifies results for this material model appearing across ranges of material constants and load levels – see [10] for more examples.

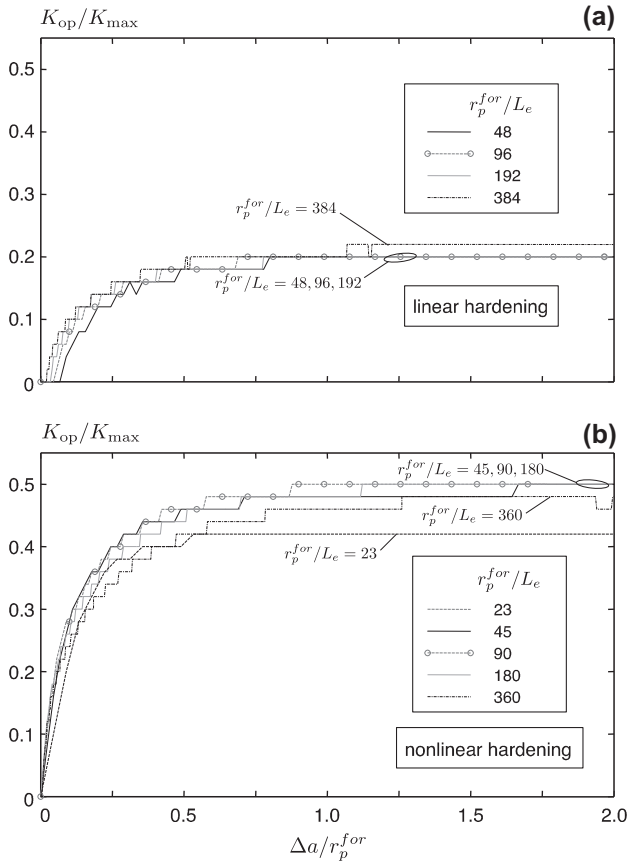

Fig. 3. Comparison of normalized opening load evolution (2nd node behind crack-tip) for different levels of mesh refinement in plane stress. Material models: (a) linear kinematic hardening and (b) nonlinear kinematic hardening. Opening loads via linear kinematic hardening model are insensitive to mesh refinement while opening loads computed via nonlinear kinematic hardening do not converge.

These analyses (and all reported in this paper) employ small strain kinematics. Roychowdhury and Dodds [3] found that small and large strain kinematics produced similar opening loads with the linear hardening material model over the considered range of mesh densities. Finer meshes can increase the influence of the kinematic formulation, generally amplifying the mesh-dependence trends for large strain analyses [10]. For consistency, data and conclusions here pertain only to small strain results.

The rationale of using the second node behind the crack tip to define the opening load levels stems from the need to measure when the crack becomes fully open while avoiding displacements from the first node behind the tip. The opening load at the first node often exhibits anomalously higher opening loads than indicated by the smooth opening behavior of the remainder of the crack face. Nevertheless, even moderate gradients in opening loads with distance from the tip render second node-based opening load comparisons among different mesh sizes inconsistent. With mesh sizes of L_e and $2L_e$, for example, the second node sits $2L_e$ and $4L_e$ behind the tip, respectively. The opening behavior as a function of physical distance from the crack tip provides a clearer picture of mesh refinement effects.

Fig. 4 records the load at which each node behind the crack tip opens during a single load cycle for both the linear and nonlinear hardening material models. The figure compares opening load values from different levels of mesh refinement, aligned by distance from the crack tip and normalized by the size of the initial forward plastic zone. The size of the initial forward plastic zone is independent of element mesh at these levels of refinement, but differs slightly for the two material models. In Fig. 4a, the linear hardening model produces monotonically convergent opening loads with mesh refinement. Moreover, this distance-based view of near-tip opening loads reveals that numerical convergence requires on the order of 190 elements defined in the forward plastic zone. The coarser meshes exhibit significantly more element size sensitivity here than is apparent in Fig. 3a.

For the nonlinear hardening material, this distance-based comparison also highlights greater mesh size sensitivity than does consideration of only the second node Fig. 3b. Here, opening loads decrease monotonically with mesh refinement over a significant portion of the crack wake. Unlike the linear hardening model, however, opening loads for the nonlinear model show no signs of converging. Even though the finest mesh has 360 elements in the initial plastic zone, mesh refinement continues to reduce the opening loads.

4.2. Mesh independence for stationary cracks

Despite the marked difference in the element size dependence of opening loads for the linear and nonlinear hardening material models, mesh refinement of stationary cracks produces remarkably similar effects for both material models. Fig. 5 demonstrates strong mesh independence of the opening profile for both models, even at small distances behind the crack tip. For increased clarity, the figures in this section employ absolute units rather than the relative units of the previous section. The three meshes here correspond to the coarsest three meshes in the above section, *e.g.*, L_e = 10 μm produces 48 and 45 elements in the initial plastic zone for the linear and nonlinear hardening models, respectively.

Fig. 5a and b depicts opening profiles at the peak of the first and tenth load cycles, respectively. The first few nodes behind the crack tip ($r = 0$) necessarily show some element size effects due to the strong curvature of the opening profile. Nevertheless, both materials display a unique opening displacement profile – finer meshes place additional nodes on the same curve nearer to the tip. The softer response of the nonlinear hardening model at large plastic strains leads to the more blunted profile near the tip. In the first

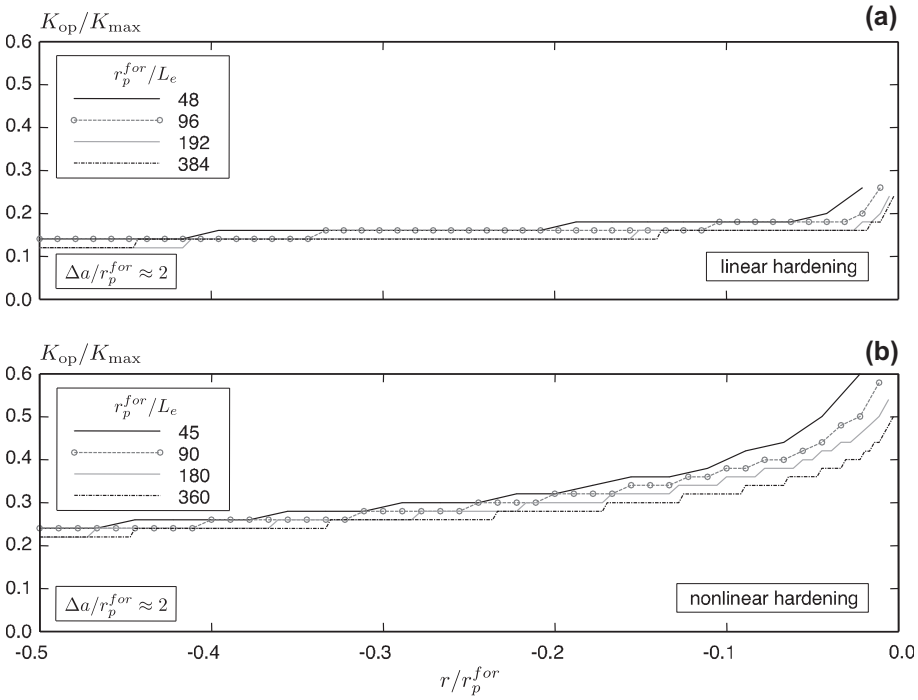

Fig. 4. Comparison of normalized opening loads by physical distance from current crack-tip for different levels of mesh refinement in plane stress. Material models: (a) linear kinematic hardening and (b) nonlinear kinematic hardening. Opening loads via linear kinematic hardening model converge with mesh refinement while opening loads computed via nonlinear kinematic hardening do not.

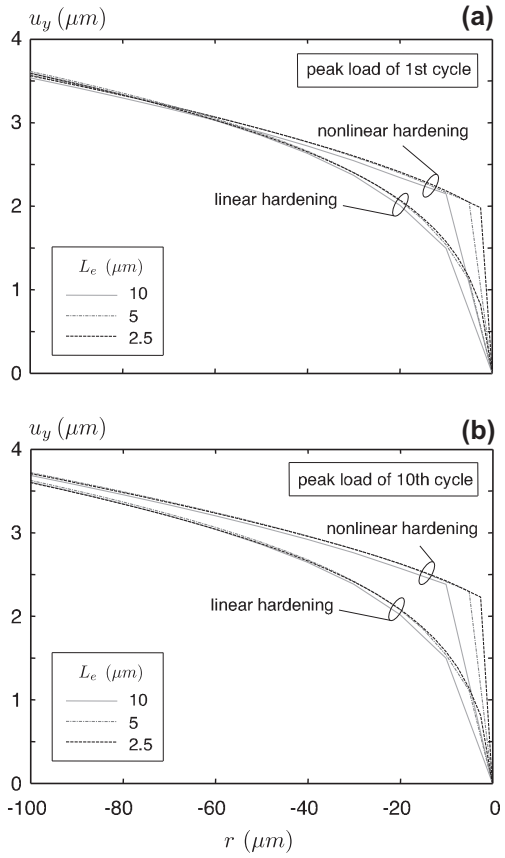

Fig. 5. Comparison of opening profile at maximum load for different levels of mesh refinement. Stationary crack in plane stress. Material models: (a) linear kinematic hardening and (b) nonlinear kinematic hardening. Both models produce displacements insensitive to mesh refinement but only the nonlinear kinematic hardening model leads to cycle dependence.

load cycle, at 60 μm behind the tip, the opening profiles are the same for both materials. Repetitive load cycling widens the opening profile with the nonlinear hardening model but not with the linear hardening model. Even though the displacement profile of the nonlinear hardening model changes with continued cycling, it remains mesh independent at these levels considered.

The opening stress profiles provide further insight into element size and load-cycle sensitivities with the linear and nonlinear hardening models. Fig. 6 presents opening stress distributions along the crack plane ahead of the crack tip at maximum load for the first and tenth load cycle of the stationary crack. Each graph shows stress values from three meshes with different levels of refinement. Again, the stationary crack tip is at $r = 0$.

Fig. 6a and b shows stresses for the linear hardening model. The stresses reveal mesh independence over most of the crack plane although the peak stress increases sharply with mesh refinement. The linear hardening model here has $E_T = 0.2E$, and thus produces significant hardening leading to a stress field having a near singularity. As such, the finer meshes resolve higher opening stresses since they have Gauss points nearer the crack tip. Most significantly, opening stresses for the linear hardening model remain unchanged by the number of load cycles.

The nonlinear hardening material model (Fig. 6c and d) produces markedly different stress distributions. The opening stress distributions exhibit strong mesh independence, even directly ahead of the crack tip because the nearly perfectly plastic behavior at large strains limits the attainable stress levels (these are plane stress solutions). Nevertheless, the monotonic and cyclic stress distributions are significantly different. At the peak of load cycle one, the stresses form a plateau ahead of the crack tip and gradually transition to lower, linear-elastic stress levels away from the tip. Under cyclic loading, a strong depression develops within this otherwise monotonic plateau region due to stress relaxation. As found for the crack opening displacements, opening stresses for the nonlinear hardening model evolve with cyclic loading but remain mesh independent for the stationary crack.

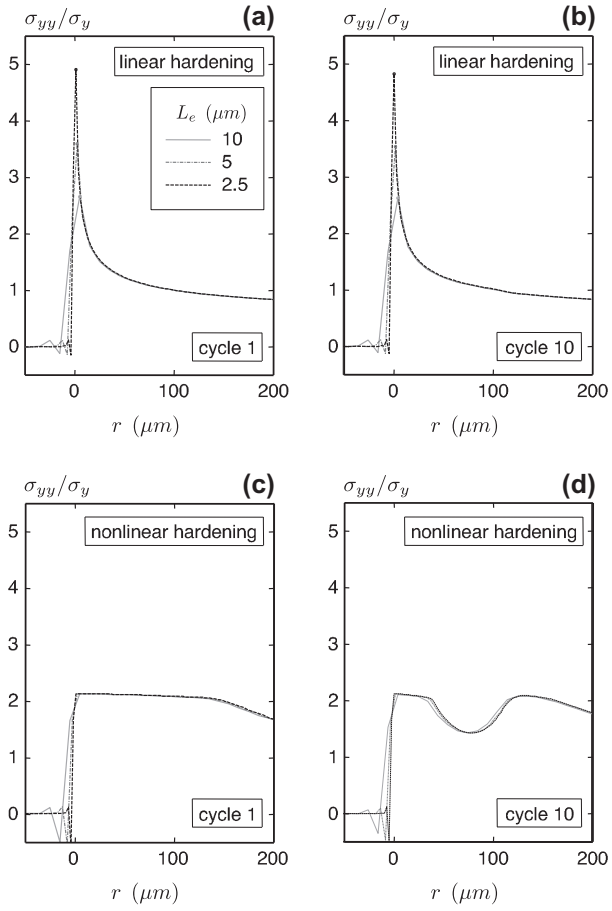

Fig. 6. Comparison of opening stress at maximum load for different levels of mesh refinement. Stationary crack in plane stress. Material model and load cycle: (a) linear kinematic hardening, cycle 1, (b) linear kinematic hardening, cycle 10, (c) nonlinear kinematic hardening, cycle 1, (d) nonlinear kinematic hardening, cycle 10. The linear hardening model produces slight mesh sensitivity at the crack-tip but no cyclic changes. The nonlinear hardening model leads to mesh-insensitive but cycle dependent opening stresses.

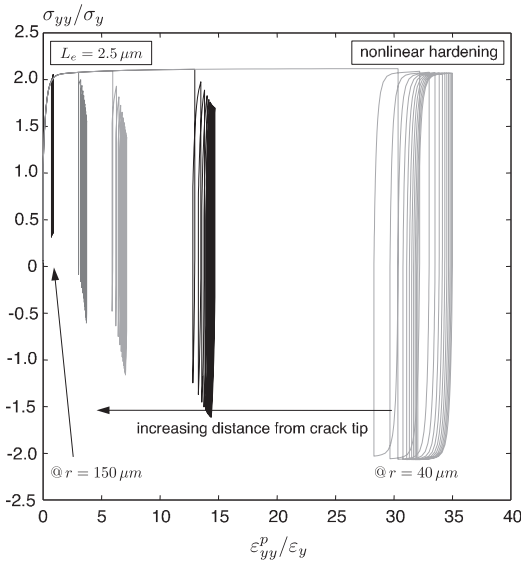

Fig. 7. Stress–plastic strain history at various near crack-tip locations along the crack plane for a plane stress stationary crack with nonlinear kinematic hardening. Both ratcheting and stress-relaxation occur, with magnitudes depending on distance from crack-tip.

4.3. Plastic zone stress relaxation and strain ratcheting with nonlinear kinematic hardening

For the plane-stress, stationary crack model, the stress–plastic strain curves in Fig. 7 demonstrate the stress relaxation and strain ratcheting effects with the nonlinear kinematic hardening material model. At material points within the plastic zone, the stress and plastic strain normal to the crack plane evolve as shown with the uniform remote load cycles ($R = 0$). The nature and degree of effects from load cycling on the stress–strain response vary with the proximity of the material point to the crack tip. The location nearest the tip ($r = 40$ μm) exhibits significant strain ratcheting, but little stress relaxation. The intermediate distances, within the depression seen in Fig. 6, exhibit both ratcheting and relaxation with magnitudes that vary with distance from the tip. Further away from the tip, the material undergoes cyclic hardening with slight amounts of ratcheting.

Fig. 8 examines the opening stress distribution near the crack tip at peak load, as in Fig. 6, but compares the effects of load cycle number rather than mesh size. The stress distributions correspond to different load cycles of one stationary crack analysis with the nonlinear hardening material model. Strong cyclic effects continue over many load cycles and vary with distance from the crack tip.

Fig. 9 appears very similar to the previous figure but the stress values derive from crack growth analyses – not stationary crack solutions. The opening stress distributions reflect those at the peak load for different levels of mesh refinement with programmed crack growth of one element per cycle instead of a single mesh with a cyclically loaded but stationary crack. The different curves represent different element sizes. For all meshes, the stresses correspond to the same amount of crack growth such that the final crack tip location lies outside of the initial plastic zone. Note that since the crack grows by one element per cycle, different element sizes require different numbers of load cycles to reach the same amount of crack growth. For example, the coarsest and finest mesh require 25 and 400 cycles respectively to grow the crack to the same final length of $\Delta a/r_p^{for} = 1.1$. Development of the stress relaxation induced depression in normal stress with decreasing mesh size here matches that due to repetitive cycling without crack growth.

For the nonlinear hardening model, the combination of Figs. 6 and 9 reveals that the crack growth procedure leads to element size dependent stress–strain fields. For a stationary crack, opening stresses are mesh independent but change with repetitive load cycling. The "standard" crack growth procedure ties the number of load cycles that a location ahead of the crack tip experiences over the course of the analysis to the element size. The computational crack-growth rate – the amount of crack extension per load cycle – decreases with decreasing element size. Thus cyclic changes in stresses and strains accumulate in distinctly different ways for varying levels of mesh refinement due to discrepancies in the crack-growth rate.

4.4. Strain ratcheting under plane strain with linear hardening material model

The previous section demonstrates the strong cyclic effects in plane stress conditions of stress relaxation and strain ratcheting inherent in the nonlinear hardening model leading to mesh dependence when the crack growth rate depends on the element size. The current section illustrates that in plane strain ratcheting can occur in the crack-tip plastic zone for simple linear (kinematic) hardening and for elastic–perfectly plastic material models, thus

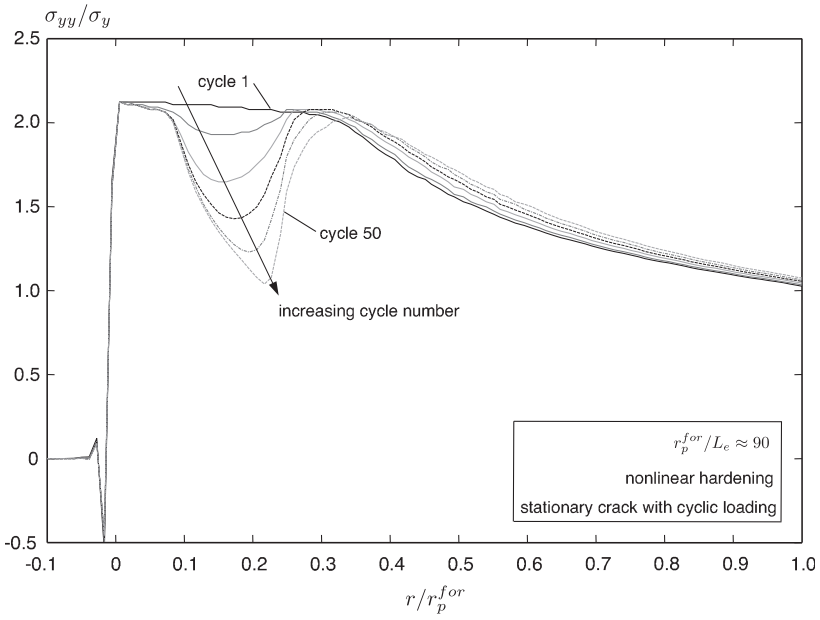

Fig. 8. Evolution of opening stress at maximum load for stationary crack with cyclic loading in plane stress, nonlinear kinematic hardening. The stress profile changes with each additional load cycle, including a severe stress-relaxation induced depression near crack-tip.

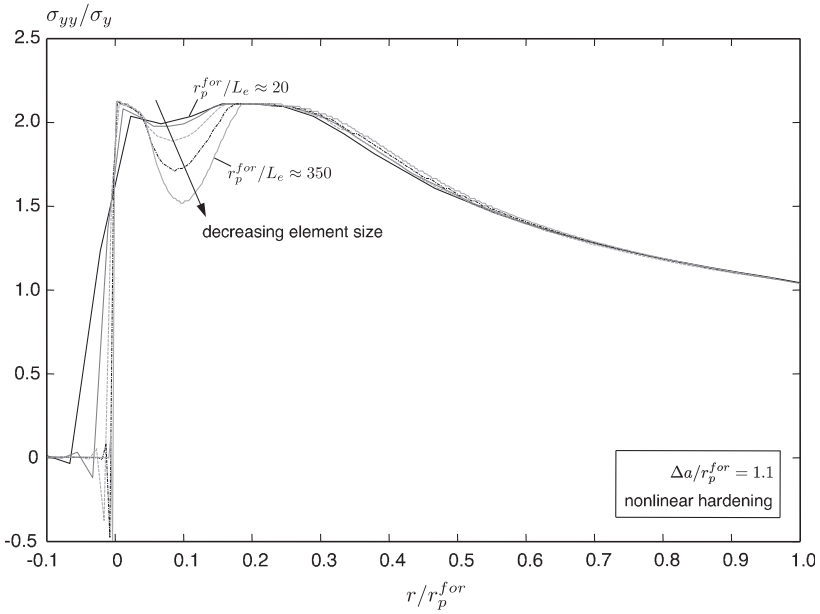

Fig. 9. Comparison of opening stress at maximum load for different levels of mesh refinement. Growing crack in plane stress, nonlinear kinematic hardening. Lines correspond to different meshes but amount of crack growth is constant across all analyses. Finer meshes exhibit stress-relaxation effects comparable to those seen for cyclic loading of a stationary crack.

leading to the same source of mesh dependence in crack opening loads.

4.4.1. Non-hardening material model

Extensive ratcheting occurs with the elastic–perfectly plastic material model in plane-strain crack analyses. Fig. 10 compares the opening stress–strain history for the nonlinear hardening material model in plane stress and the elastic–perfectly plastic model in plane stress and plane strain. These stress–strain histories refer to the center of the element directly ahead of the stationary crack tip; the mesh is identical for all three analyses. The remote, displacement-controlled loads impose 20 cycles with 100 uniform load increments per cycle. In plane stress, the additional increments of strain ratcheting diminish steadily with repeated cycling of the nonlinear hardening model. The elastic–perfectly plastic model, in plane stress, creates large opening strains but essentially no further ratcheting after the second cycle. The elastic–perfectly plastic model in plane strain generates much smaller opening strain on the first cycle. However, ratcheting increases the opening strain by over $6\varepsilon_y$ in the first cycle and still contributes nearly an additional $4\varepsilon_y$ increment in the 20th cycle for a total strain accumulation of $96\varepsilon_y$ over the 20 cycles, where ε_y is the strain at yield onset in monotonic uniaxial loading.

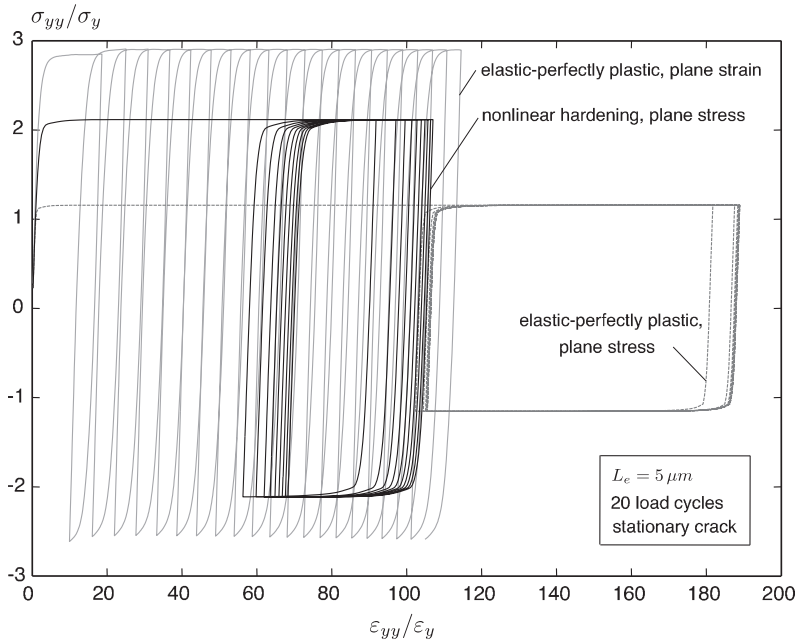

Fig. 10. Stress–plastic strain history at center of element ahead of stationary crack-tip under cyclic loading for nonlinear kinematic hardening in plane stress and linear kinematic hardening in both plane stress and plane strain. The linear hardening model ratchets strongly in plane strain but not in plane stress. The nonlinear hardening model produces ratcheting also, but the magnitude decreases sharply with continued load cycling.

The strain ratcheting affects the opening displacements (see Fig. 5) for the nonlinear hardening model in plane stress. With that material model, opening displacements of the stationary crack increase with repeated load cycling in a smooth manner along the crack face [the increased mesh refinement indicated in the figure resolves details of a realistic, blunting shape immediately at the tip but otherwise has no effect]. Fig. 11a shows the opening profile of the stationary crack for the elastic–perfectly plastic model in plane stress and plane strain. For plane-stress conditions, opening displacements do not change with load cycling since the material model does not generate ratcheting strains. In sharp contrast, repetitive load cycles of the stationary crack in plane strain for the elastic–perfectly plastic material generate a strong but very localized effect on the opening profile. Each additional load cycle sharply increases the opening displacement at the first node behind the crack tip creating an unrealistic "pinched" profile. Load cycling also affects displacements at the next four nodes behind the crack tip, but opening displacements at greater distances from the crack tip remain unaffected.

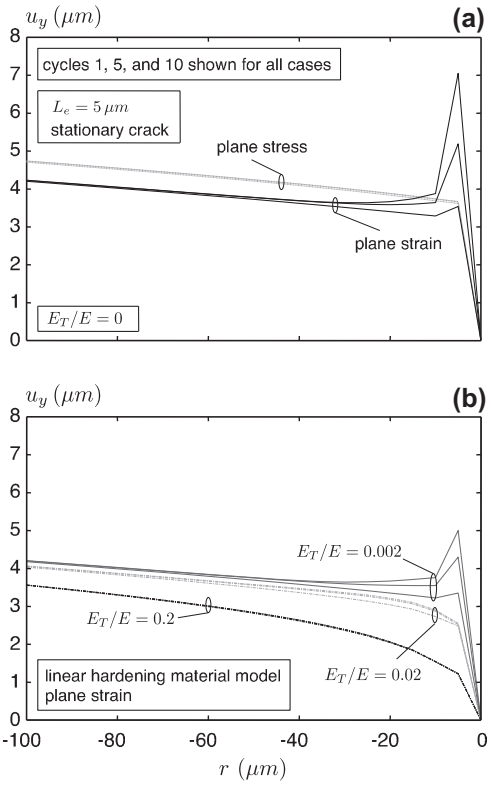

Fig. 11. Crack opening profile at maximum load for stationary crack under cyclic loading: (a) elastic–perfectly plastic material behavior in plane stress and plane strain, and (b) linear kinematic hardening with different levels of strain hardening.

4.4.2. Plastic modulus effects with linear hardening material model

Continuing with the plane-strain solutions of the stationary crack model, Fig. 11b demonstrates the strong sensitivity of cyclic changes in opening displacement, including the unrealistic localized deformation at the tip, to the plastic modulus. An increased plastic modulus decreases the ratcheting strains in each cycle thereby suppressing development of the pinched profile. A moderate amount of hardening, $E_T/E = 0.02$, essentially eliminates the pinching deformation.

Fig. 12 further correlates plane-strain ratcheting and localized deformations leading to the pinched profile. The opening stress–plastic strain history shown for the center of the element directly ahead of the stationary tip demonstrates the accumulation of plastic strain via ratcheting over 10 load cycles. The inset drawings show deformed meshes around the crack tip at peak load of the tenth cycle. For an elastic–perfectly plastic material in plane strain ($E_T/E = 0$), ratcheting strains become extensive and very slow to saturate with continued cycling. The first node behind the crack tip exhibits excessive displacement caused directly by large ratcheting strains in the crack-tip element. The intensity of pinching decreases steadily with increasing plastic modulus. This corre-

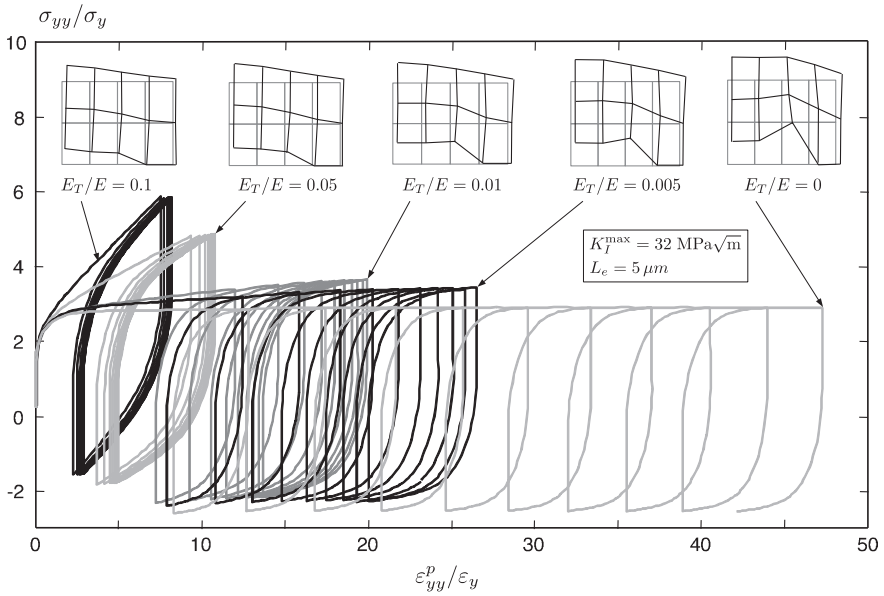

Fig. 12. Plane strain stress–strain hysteresis and mesh deformation near stationary crack-tip for the linear kinematic hardening model with different levels of strain hardening. Deformed mesh at the peak load of the 10th cycle shown relative to undeformed mesh.

sponds to a marked decrease in the magnitude of ratcheting strains and the smaller number of cycles required to approach saturation (no further increments of ratcheting strain). Nevertheless, even rather high moduli ($E_T/E = 0.1$) produce some ratcheting in plane strain.

This section reveals the development of extensive ratcheting strains for low plastic modulus and non-hardening material models under plane-strain conditions. The corresponding, unrealistic "pinched" opening profile affects directly the crack opening computations since most methods for determining the opening load rely on the displacement of nodes near the crack tip. Further, strain ratcheting causes the the opening loads to exhibit element size dependence for analyses in which the element size sets the simulated rate of crack growth. Indeed, even the existence of crack closure in plane strain is controversial, with some numerical studies suggesting that closure does not occur (see [9] and references therein for further discussion). The current study demonstrates that linear hardening models can have serious numerical shortcomings in plane strain for cyclic loading, including non-physical crack opening profiles and un-realistic ratcheting strains that do not saturate. This may be the source of conflicting results for plane-strain crack opening loads reported in the literature.

4.5. Number of load cycles between node release events

The previous sections establish that certain combinations of material models and constraints (plane stress, plane strain) lead to strain ratcheting. In such models, the opening behavior of a growing crack exhibits mesh dependence due to the link between element size and the computational rate of crack growth. The rate of crack growth also depends on the number of cycles imposed between node release events. This section examines how the number of load cycles between node releases alters the opening profile and plastic strain accumulation for plane strain analyses with the linear hardening model and with elastic–perfectly plastic behavior. *Opening profiles* Fig. 13 demonstrates the impact of load cycling between node releases on changes in the opening profile at peak load for both a non-hardening and linear hardening material. For each material model ($E_T/E = 0$ in Fig. 13a and $E_T/E = 0.05$ in Fig. 13b), opening displacements correspond to three separate analyses during which node release occurs every cycle (nr1), every fifth cycle (nr5) or every tenth cycle (nr10). Analyses with multiple load cycles between node releases report the opening profile at the peak load of the first cycle after node release and the last cycle before the next node release.

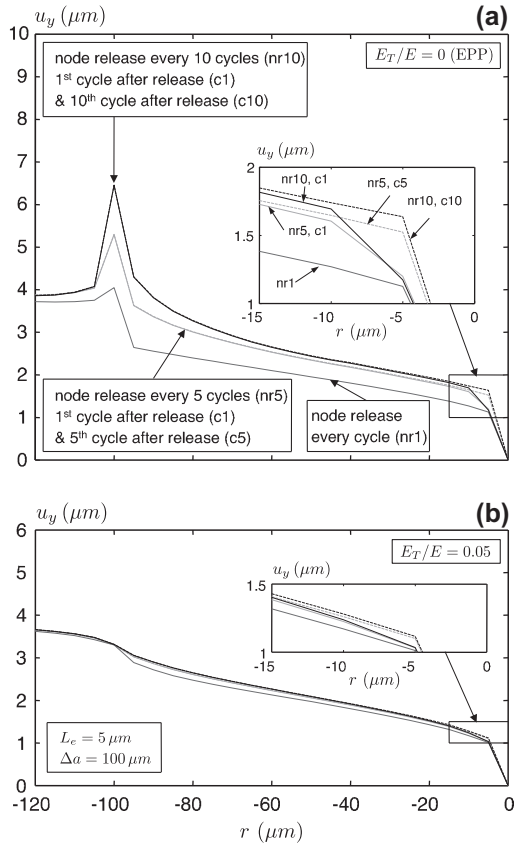

Fig. 13. Crack opening profile at maximum load when $\Delta a \approx$ 100 μm for three different node release schemes. Material model: (a) elastic–perfectly plastic and (b) linear kinematic hardening with $E_T/E = 0.05$.

In Fig. 13a, the sharp peak at $r = -100$ μm corresponds to the crack-tip location before any growth. This pinched profile sharpens with increasing number of cycles prior to the first node release. This is the effect of load cycling on a stationary crack seen previously in Fig. 11. Intermediate distances from the current crack tip, $-20 < r < -80$ μm, exhibit large differences in peak opening displacement using 1 or 5 cycles between node releases. This effect decreases, but still exists, on increasing from 5 to 10 cycles between node releases. The opening displacement of the first node behind the tip in the first cycle after node release remains unaffected by the number of cycles between releases – see inset of Fig. 13a. This produces a somewhat rounded profile for the solutions with 5 and 10 cycles per node release. For more load cycles without crack growth, the displacement at the first node increases to match the remainder of the nodes.

In Fig. 13b, for $E_T/E = 0.05$ the opening profile becomes quite smooth (even near the initial tip). Increasing the number of load cycles between node release has much less influence on the displacements than in the elastic–perfectly plastic case. Only a relatively small difference exists between the solutions with 1 cycle and 5 cycles per node release. The 5 and 10 cycle analyses are essentially identical because the ratcheting strains effectively saturate for this level of plastic modulus and the number of cycles ($\geqslant 5$).

Fig. 13 apparently indicates that the sharp peak ("pinch") in displacements for models with a low plastic modulus occurs only at the initial tip, regardless of the number of load cycles between node release. However, with further growth suspended at some point in an analysis, the application of more load cycles – beyond the number of load cycles between node releases employed while growing the crack to the current length – creates yet another sharp pinch in displacements at the node directly behind the crack tip. For the elastic–perfectly plastic material, simply one more cycle on a suspended crack tip causes the peak opening displacement at node 1 to be greater than at node 2. The effect, though less dramatic, exists for $E_T/E = 0.02$, but essentially vanishes for $E_T/E = 0.05$. Thus, while the profile for a growing crack may appear well-behaved in analyses with *uniform* loading history, variable load cycling patterns including overloads may cause unrealistic displacement localization (pinching) of the type illustrated here.

4.5.1. Plastic strain distributions

As shown above, the number of load cycles between node releases influences the plane-strain opening displacements for a non-hardening material more than for a hardening material. This follows directly from the relationship between the plastic modulus and the generation of ratcheting strains. To clarify and expand on the role of load cycles, Fig. 14 examines the evolution of plastic opening strain in the 18th element ahead of the initial crack tip as the advancing crack tip approaches and passes this element. After the 17th node release, this element lies directly ahead of the tip; after node release 19 it lies two elements behind the tip (in the crack wake). The data here align by node release events for clarity. For analyses with 5 cycles and 10 cycles per node release, there are 5 and 10 complete load cycles shown between each whole number on the abscissa, respectively. The figure omits the first 13 node releases for space and scaling reasons.

For the non-hardening model (Fig. 14a), more load cycles between crack-growth increments produce more ratcheting at the beginning of the analysis (not shown). For the three loading protocols shown, no reverse yielding (decreasing ε^p_{yy}) occurs until the crack tip is within 20 μm (four elements); thereafter reverse yielding becomes significant. When the crack tip approaches the monitored element, additional load cycles between node releases increase the overall accumulation of plastic opening strain. Nevertheless, the per-cycle change (peak-to-peak change in plastic strain) shown in the figure is largest for the protocol with node release every cycle.

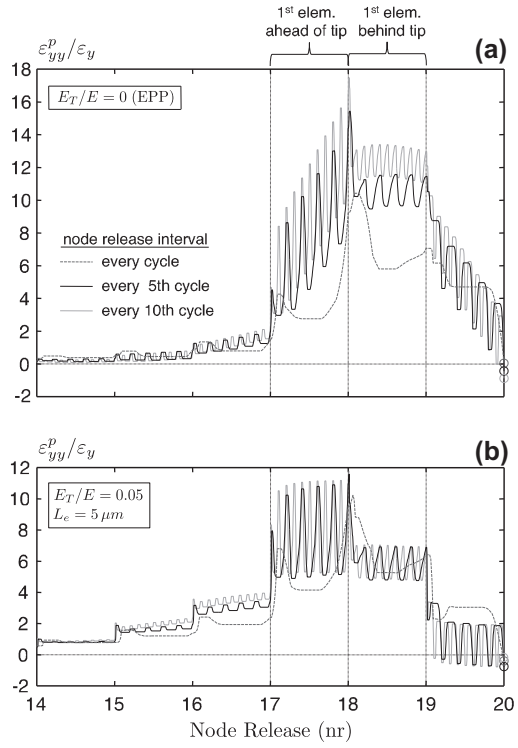

Fig. 14. Plastic strain accumulation for growing crack in plane strain at ≈90 μm ahead of initial crack-tip. Material model: (a) elastic–perfectly plastic and (b) linear kinematic hardening with $E_T/E = 0.05$. Open circles at $nr = 20$ emphasize the residual plastic strain just before the 20th node release: for the elastic–perfectly plastic model the plastic strain is compressive for both the 5 and 10 cycle protocols but slightly tensile for node release every cycle. For the linear hardening case, the plastic strain is compressive for all three analyses.

The node release protocol remains important after the crack tip moves beyond an element. The plastic strains maintain significantly higher levels for multiple load cycles between node release while the monitored element here lies immediately behind the tip. When the crack advances again and the monitored element becomes the second from the tip in the crack wake (19–20 increment on the abscissa), plastic strain increments in the reverse (compressive) direction accumulate more for analyses with more cycles between node release. Right before the 20th node release, when the monitored element continues as the second element behind the tip, the current plastic strain (ε^p_{yy}) remains slightly tensile for the protocol with node release in every cycle. For the other two node release protocols, the plastic strain becomes compressive and the magnitude for the 10 cycle release is twice that for the the 5 cycle release ($\varepsilon^p_{yy} = -0.0032$ and -0.0016, respectively).

The plastic strain history for the hardening material (Fig. 14b) differs notably from the non-hardening material. As the crack tip approaches, the plastic opening strain is slightly higher for $E_T/E = 0.05$ than for the elastic–perfectly plastic material. For the hardening material, the node release protocol has a somewhat larger influence on strain accumulation for node release intervals 15–16 and 16–17 but much less effect when the element lies directly behind the tip, and as the tip moves beyond the monitored element at node release 18. The analyses using 5 and 10 cycles per release produce very similar plastic strain histories which differ significantly from that of the 1 cycle per release analysis. This again demonstrates that ratcheting effectively saturates with sufficient cycles between node releases for sufficiently large values of the plastic modulus.

The number of load cycles imposed between node releases induces both immediate (crack tip approaching) and longer-term (crack tip has passed) impacts on the opening displacements and stress–strain fields. Nevertheless, the compensating effects of forward and reverse yielding reduce the effects of load-cycles-per-release in the wake of a growing crack compared to the conditions of a stationary crack which generate only forward yielding: (a) the increased forward plastic strain in elements ahead of the crack tip actually reduces the closure load by widening (blunting) the opening profile; (b) the same forward plastic strain in those elements after they move into the crack wake manifests as residual material along the crack face which tends to increase closure loads. Ratcheting increases the plastic strain in front of the tip while reducing the plastic strain in the wake through reverse (compressive) yielding when the crack is closed. The *net* effect observed here for the growing crack becomes somewhat counter-intuitive: more load cycles tend to produce less closure (smaller opening loads). McClung and Sehitoglu [27] observed this phenomenon and described it in terms of decreasing mean stress with more load cycles per node release leading to sharp decreases in open stresses.

This section demonstrates that the node release protocol, *i.e.*, the number of load cycles between crack advancements, can play a large role in the shape of the opening profile and the evolution of plastic strain. The strength of this effect depends strongly on the cycle sensitivity in the material model. The strongly ratcheting, perfectly-plastic material model in plane strain produces opening profiles and plastic strain histories that continue to show protocol dependence even for 10 load cycles between node releases. In contrast, the protocol effects saturate with fairly small numbers of load cycles between crack advancements if the plane strain analysis employs a moderate amount of linear hardening ($E_T/E = 0.05$). This section also reveals the competing effects of load-cycles-per-release on forward and reverse plastic strain such that more load cycles actually leads to lower opening loads due to decreased residual strain in the plastic wake.

4.6. Growth rate effect on opening loads

The previous sections establish the connection of the enforced computational crack-growth rate, the opening displacement and the stress–strain evolution for materials and constraints (plane stress, plane strain) that produce ratcheting. The computational crack growth rate depends on both the element size and the number of load cycles between crack advancements. Mesh refinement studies in plasticity induced crack closure modeling often do not vary the number of load cycles. As such, the rate of crack growth decreases with decreasing mesh size and thus finer meshes experience more load cycles. By adjusting the number of cycles between node releases, the analyst can enforce equal rates of crack growth across different levels of mesh refinement.

Fig. 15 again confirms that non-convergence with mesh refinement arises primarily from this issue of computational crack-growth rates. Fig. 15a presents the opening loads at nodes behind the crack tip during one load cycle for three increasing levels of mesh refinement. For each mesh, the crack grows by one element size in each load cycle. These analyses use the nonlinear kinematic hardening model in plane stress. The finest mesh employs elements 1/16th the size of those for the coarsest mesh. Correspondingly, the crack advances in the finest mesh at 1/16th the rate of the coarsest mesh. The figure confirms that the opening loads decrease sharply with mesh refinement.

The analyses in Fig. 15b enforce the same computational growth rate for all three meshes. For the finest mesh, the opening loads are unchanged from Fig. 15a and define the reference growth rate (using 1 cycle per node release). For the intermediate and coarsest meshes, analyses in Fig. 15b have 4 and 16 load cycles per node release, respectively. The opening load distributions for the three meshes shown using physical distances from the crack tip now agree remarkably well. A node-based comparison of opening displacements very near the tip continues to exhibit mesh dependence as the physical position of the second node depends on the element size and the opening loads vary with distance from the crack tip.

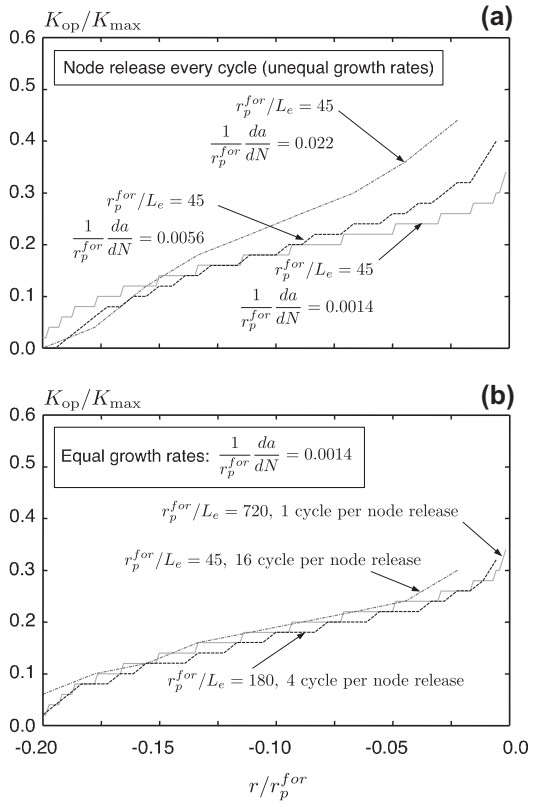

Fig. 15. Comparison of normalized opening loads by distance from current crack-tip for nonlinear kinematic hardening in plane stress: (a) node release every cycle such that the levels of mesh refinement produce different simulated crack-growth rates and (b) equal simulated crack growth rates among the three level of mesh refinement due to element-sized based load cycling between node release.

Fig. 15 both illustrates the source and a means to ameliorate non-convergence of opening loads with mesh refinement. However, it also highlights a fundamental issue in the conventional approach to model fatigue crack growth with finite element analyses — opening loads can be growth-rate dependent for material models and constraints that produce cyclically evolving stress–strain response (*e.g.*, ratcheting).

5. Summary and conclusions

This paper investigates the coupled role of strain ratcheting and load cycling on the mesh dependence often observed in opening loads, opening profiles and stress–strain fields computed in finite element analyses of plasticity induced crack closure. The finite element analyses illustrating these effects here employ a mode I, small-scale yielding boundary-layer framework in both plane stress and plane strain, with non-hardening, linear kinematic hardening, and nonlinear kinematic hardening elastic–plastic constitutive models. The specific observations and conclusions of this work apply to small-strain formulation, 2D models with zero *T*-stress and $R = 0$ constant amplitude loading. Analyses of a stationary crack under cyclic loading provide reference solutions to first examine sources of potential mesh dependencies. Crack-growth

analyses under cyclic loading adopt the common approach of programmed node release at pre-defined points in the cyclic loading history. The element size and number of cycles between node release thus couple to set the crack-growth rate in the computational model. The different load histories experienced at material points ahead of the crack tip imposed by these selections in the finite element model lead to computed differences in opening profiles and near-tip stresses.

For a stationary crack subjected to cyclic loading under plane-stress and plane-strain conditions, the linear and nonlinear hardening models generate near-tip fields and crack-opening profiles that converge with mesh refinement. Solutions with the nonlinear hardening model reveal crack-tip fields strongly sensitive to the loading history, but in a non-mesh dependent manner. For crack growth under plane-stress conditions by programmed node release during cyclic loading, mesh refinement with the linear hardening model leads to convergent opening loads while the nonlinear hardening model exhibits strongly non-convergent opening behavior. In plane stress, the load paths of material points in the crack-tip region remain proportional during plastic flow with linear kinematic hardening or perfect plasticity. Thus the plastic tangent operator does not depend on the stress state (as the appendix demonstrates) and no ratcheting occurs. Nonlinear kinematic hardening ratchets under any non-symmetric loading including proportional paths.

Under plane-strain conditions, the linear hardening model (with a low or zero plastic modulus) and the nonlinear hardening model both reveal a cycle dependence and mesh dependence for a growing crack. In plane strain, evolution of the out-of-plane stress leads to non-proportional plastic flow in general, even for the elastic–perfectly plastic model in uniaxial plane strain (refer to appendix). This non-proportionality creates a stress–state dependence in the plastic tangent operator which causes ratcheting for certain ranges of applied loading and plastic moduli.

The following list summarizes more specific observations/conclusions of the present work on the mesh and cycle dependence of fatigue crack analysis.

1. Mesh dependence in 2D PICC finite element analysis occurs frequently in convergence studies reported in the literature. The common assumption of adequate mesh refinement having ten elements in the forward plastic zone in general *does not* hold. The present work confirms the existence of non-convergent opening loads with element mesh refinement for certain choices in the continuum-level problem specification (*e.g.*, material model, plane stress *vs.* plane strain).
2. For a stationary crack, computed crack-tip field quantities (displacement and strains–stresses) reveal converged solutions with mesh refinement, but may have a load cycle dependence. Under monotonic loading, fields converge with mesh refinement for linear and nonlinear hardening models in both plane stress and plane strain. Cyclic loading (without crack growth) also produces convergent crack-tip fields with mesh refinement for linear and nonlinear (kinematic) hardening models in both plane stress and plane strain. Displacements and strains–stresses continue to evolve with repeated load cycling for: (a) nonlinear hardening models in plane stress and plane strain, (b) elastic–perfectly plastic materials in plane strain, and (c) linear (kinematic) hardening models for materials having a small value of the plastic modulus in plane strain. In plane stress, displacements and strains–stresses do not evolve (or they saturate quickly) under continued cyclic loading for the linear (kinematic) hardening model with all values of the plastic modulus including zero.
3. Strain ratcheting leads to mesh dependence of the crack-tip fields and the opening loads in analyses with crack growth for: (a) nonlinear (kinematic) hardening material models in plane stress and in plane strain; and (b) elastic–perfectly plastic materials and linear kinematic hardening models with a small plastic modulus in plane strain. The link between crack-growth rate and element size implicit in the crack-growth procedure using node release is responsible for this mesh dependence – different element sizes require different numbers of load cycles to produce the same amount of crack growth.
4. Several conditions affect the amount and nature of strain ratcheting and thus the manifestation of mesh dependence. Material model: the nonlinear kinematic hardening model ratchets for non-symmetric load cycles; the linear kinematic hardening model ratchets for some non-proportional load paths, including crack-tip conditions that exist under plane-strain conditions. The linear hardening model does not ratchet under proportional loading, including crack-tip conditions of plane stress. Material flow properties: smaller plastic moduli lead to more ratcheting. Plane stress *vs.* plane strain: plane strain generally produces more ratcheting than plane stress.
5. For material models and constraint conditions that activate strain ratcheting, opening loads depend on the rate of crack growth, which derives from the coupled effect of element size and the number of cycles between discrete crack growth events. Slower growth rates (finer meshes and/or more cycles between crack advance) produce more ratcheting but generally lower opening loads due to the competing effects of plastic strain ahead of and behind the crack tip and the significance of reverse plasticity.
6. When crack-opening loads reveal non-convergent behavior with levels of mesh refinement, it may be possible to adjust the number of load cycles between crack advances to achieve comparable crack-growth rates across mesh refinement levels, and thereby reduce the apparent mesh dependence of crack-opening loads. This process achieves convergent, but not necessarily physically relevant, numerical solutions. Analyses with the nonlinear kinematic hardening model in plane stress, for example, indicate solutions with the same growth rate (ratio of element size to number of load cycles between crack advance) produce essentially identical opening loads for points located at the same distance from the crack tip. Moreover, when distance-based opening loads do converge, opening loads based the second (or other integer) node behind the crack tip still exhibit element size dependence due to strong gradients in opening loads near the crack tip.

The enforced release of one element per load cycle most often simulates a crack-growth rate much higher than experienced in actual specimens/components. For material models and constraints (plane stress and/or plane strain) that produce ratcheting, this accelerated growth rate in the finite element model suppresses the amount of ratcheting strains developed. However, specific material models may produce unrealistic amounts of ratcheting, *e.g.*, elastic–perfectly plastic response in plane strain with zero *T*-stress. The excessive ratcheting magnifies the sensitivity of the opening load levels to the imposed computational growth rate, *i.e.*, the combination of mesh refinement and load cycles between crack advance. These observations suggest that some prior studies of PICC may reflect an implicit, element size sensitivity caused by variable (unknown) amounts of strain ratcheting. Moreover, a universal rule for element size relative to the plastic zone size *does not apply* when strain ratcheting occurs. To achieve stable and accurate opening load measurements, numerical studies need to consider the interaction of: (1) cyclic constitutive response, especially how much and over how many cycles ratcheting occurs under specific loading conditions, (2) the simulated crack-growth rate as a function of element size and load cycles per crack advancement, and (3) the spatial variation of opening load.

Acknowledgments

The Department of Energy provided funding for this work through the Computational Science Graduate Fellowship. Additional support was provided by the NASA Marshall Space Flight Center through Grant NNM04AA37G (MSFC, Mr. D.N. Wells, Technical Monitor), and by the M.T. Geoffrey Yeh Fund at the University of Illinois. The information presented in this paper is the sole opinion of the authors and does not necessarily reflect the views of the sponsoring agencies. We also thank Dr. James Sobotka for his help with the figures.

Appendix A. Ratcheting with the linear kinematic hardening material model

The linear kinematic hardening model does not ratchet for proportional applied loading, including uniaxial loading. As such, ratcheting does not exist as a "feature" of the linear kinematic hardening model. Nevertheless, the linear kinematic hardening model can produce significant strain ratcheting in non-proportional loading, especially for small values of the plastic modulus.

Ratcheting may occur whenever the tangent operator ($\partial\boldsymbol{\sigma}/\partial\boldsymbol{\varepsilon}$) depends on the current stress state. In this situation, even small differences in the magnitude of the maximum and minimum stress states can produce significantly different strain magnitudes leading to plastic strain accumulation with each cycle.

The governing equations for the linear kinematic hardening model are given below. Quantities denoted by $\|\ ()\ \|$ indicate the tensorial norm,

$$\|()\| = \sqrt{()_{ij}()_{ij}} \tag{A.1}$$

The deviatoric stress and deviatoric strain tensors, $\boldsymbol{s}$ and $\boldsymbol{e}$, follow from the stress and strain tensors, $\boldsymbol{\sigma}$ and $\boldsymbol{\varepsilon}$, respectively by

$$\boldsymbol{s} = \boldsymbol{\sigma} - \frac{1}{3}tr(\boldsymbol{\sigma})\boldsymbol{I} \tag{A.2}$$

$$\boldsymbol{e} = \boldsymbol{\varepsilon} - \frac{1}{3}tr(\boldsymbol{\varepsilon})\boldsymbol{I} \tag{A.3}$$

The backstress tensor, $\boldsymbol{\alpha}$, defines an internal variable that represents translation of the yield surface. Defining the relative stress as $\boldsymbol{\xi} = \boldsymbol{s} - \boldsymbol{\alpha}$, the elastic domain comprises all states for which $f < 0$ where

$$f = \|\xi\| - \sqrt{\frac{2}{3}}\sigma_y \tag{A.4}$$

Let $\dot{\boldsymbol{e}}^{\mathrm{p}}$ be the rate of plastic strain based on decomposition of the total strain into elastic and plastic parts, $\boldsymbol{e} = \boldsymbol{e}^{\mathrm{e}} + \boldsymbol{e}^{\mathrm{p}}$.

The plastic strain rate direction lies normal to the yield surface (associative flow rule) with magnitude determined by the consistency parameter, $\dot{\lambda}$,

$$\dot{\boldsymbol{e}}^{\mathrm{p}} = \dot{\lambda}\frac{df}{d\boldsymbol{s}} = \dot{\lambda}\frac{\boldsymbol{\xi}}{\|\boldsymbol{\xi}\|} = \dot{\lambda}\boldsymbol{n} \tag{A.5}$$

where $\boldsymbol{n}$ denotes the unit normal to the yield surface. The consistency parameter constrains stress states to the yield surface such that $\dot{\lambda}f = 0$, *i.e.*, $\dot{\lambda} > 0$ for plastic yielding and $\dot{\lambda} = 0$ otherwise.

The stress rate of change depends only on the elastic strain rate:

$$\dot{\boldsymbol{s}} = 2G\dot{\boldsymbol{e}}^{\mathrm{e}} \tag{A.6}$$

where G is the shear modulus. The back stress evolution is given by

$$\dot{\boldsymbol{\alpha}} = H\dot{\boldsymbol{e}}^{\mathrm{p}} \tag{A.7}$$

where H is a material constant that governs the slope of the post-yield response. H follows from the uniaxial tangent modulus via

$$H = \frac{EE_T}{E - E_T} \tag{A.8}$$

For the linear kinematic hardening model, the exact continuum tangent operator under plastic flow becomes

$$\frac{\partial\dot{\boldsymbol{\sigma}}}{\partial\dot{\boldsymbol{\varepsilon}}} = K(\boldsymbol{I}\otimes\boldsymbol{I}) + 2G\left[\boldsymbol{1} - \frac{1}{3}(\boldsymbol{I}\otimes\boldsymbol{I}) - \frac{2G}{2G+H}(\boldsymbol{n}\otimes\boldsymbol{n})\right] \tag{A.9}$$

where $\boldsymbol{I}$ denotes the second order identity tensor, $I_{ij} = \delta_{ij}$ and $\boldsymbol{1}$ represents the fourth order identity tensor, $1_{ijkl} = \delta_{ik}\delta_{jl}$. The tensorial modulus thus depends on the stress state via the yield surface normal, $\boldsymbol{n}$. If loading is non-proportional such that $\boldsymbol{n}$ varies, then ratcheting may occur.

Consider the case of an elastic–perfectly plastic material in plane strain, *i.e.*, $H = 0$. Let the z-direction be perpendicular to the plane of the model such that $\varepsilon_{zz} = \gamma_{xz} = \gamma_{yz} = 0$. When the material state lies in the elastic range $\dot{\sigma}_{zz} = \nu(\dot{\sigma}_{xx} + \dot{\sigma}_{yy})$.

First, consider biaxial stress-controlled loading: $\sigma_{xx} = \sigma_{yy} = \sigma(t)$, where t is a time-like parameter. Constraining plastic states to the yield surface ($f = 0$) requires

$$|\sigma(t) - \sigma_{zz}(t)| = \sigma_y \tag{A.10}$$

Yielding initiates under monotonic tensile loading when $\sigma(t) = \sigma_y/(1-2\nu)$. The out-of-plane stress becomes $\sigma_{zz}(t) = \sigma(t) - \mathrm{sgn}[\sigma(t) - \sigma_{zz}(t)]\sigma_y$, where $\mathrm{sgn}(a)$=1 if $a \geqslant 0$ and $\mathrm{sgn}(a) = -1$ if $a < 0$.

The yield surface normal has the form

$$\boldsymbol{n} = \frac{1}{\sqrt{6}}\mathrm{sgn}[\sigma(t) - \sigma_{zz}(t)]\begin{bmatrix}1 & 0 & 0\\ 0 & 1 & 0\\ 0 & 0 & -2\end{bmatrix} \tag{A.11}$$

which is independent of the stress state (within each half-cycle of monotonic loading). Thus, the strains depend linearly on the stresses and ratcheting does not occur. Now, consider the uniaxial plane-strain case defined by $\sigma_{xx} = \sigma(t)$ but $\sigma_{yy} = 0$. Plastic states are constrained such that

$$\left[\sigma^2 - \sigma\sigma_{zz} + \sigma_{zz}^2\right]^{1/2} = \sigma_y \tag{A.12}$$

where the explicit time dependence is omitted to simplify the notation.

Yielding initiates in monotonic tensile loading when $\sigma = \sigma_y/\sqrt{\nu^2 - \nu + 1}$. The out-of-plane stress is $\sigma_{zz} = 0.5\left(\sigma \pm \sqrt{4\sigma_y^2 - 3\sigma^2}\right)$, where the sign depends on the direction of loading, (-) for tensile loading and (+) for compressive loading. The theoretical maximum attainable stress is $\sigma = \sqrt{4/3}\sigma_y$ which corresponds to fully incompressible behavior (*i.e.*, $\nu \to 0.5$, $\sigma_{zz} = \sigma/2$). The yield surface normal has the form

$$\boldsymbol{n} = \frac{1}{\sqrt{6}\sigma_y}\begin{bmatrix}2\sigma - \sigma_{zz} & 0 & 0\\ 0 & -(\sigma + \sigma_{zz}) & 0\\ 0 & 0 & -\sigma + 2\sigma_{zz}\end{bmatrix} \tag{A.13}$$

which strongly depends on the stress state, even for the rather small range of attainable stress states. *Thus ratcheting can, and does occur.*

References

[1] Elber W. Fatigue crack closure under cyclic tension. Eng Fract Mech 1970;2:37–45.
[2] Newman Jr JC. A finite element analysis of fatigue crack closure. In: Mechanics of crack growth, ASTM STP 590; 1976. p. 281–301.
[3] Roychowdhury S, Dodds Jr RH. A numerical investigation of 3-d small-scale yielding fatigue crack growth. Eng Fract Mech 2003;70:2363–83.
[4] Roychowdhury S, Dodds Jr RH. Three-dimensional effects on fatigue crack closure in the small-scale yielding regime. Fatig Fract Eng Mater Struct 2003;26:663–73.

[5] Armstrong PJ, Frederick CO. A mathematical representation of the multi-axial Baushinger effect. Tech report CEGB report RD/B/N731, Berkeley Nuclear Laboratories, R&D Department; 1965.
[6] Auricchio F, Taylor RL. Two material models for cyclic plasticity: non-linear kinematic hardening and generalized plasticity. Int J Plast 1995;11:65–96.
[7] Hibbit, Karlsson & Sorensen, Inc. ABAQUS standard user's manual: version 6.3, Pawtucket, RI; 2002.
[8] McClung RC. Finite element analysis of fatigue crack closure: a historical and critical review. In: Fatigue '99: proceedings of the seventh international fatigue congress, 8–12 June, 1999, Beijing, China; 1999.
[9] Solanki K, Daniewicz SR, Newman Jr JC. Finite element analysis of plasticity-induced fatigue crack closure: an overview. Eng Fract Mech 2004;71:149–71.
[10] Cochran KB. Numerical modeling issues in finite element simulation of plasticity induced crack closure with an emphasis on material model effects. PhD thesis, University of Illinois at Urbana Champaign; 2009.
[11] McClung RC, Sehitoglu H. On the finite element analysis of fatigue crack closure – 1. Basic modeling issues. Eng Fract Mech 1989;33:237–52.
[12] McClung RC, Davidson DL. High resolution numerical and experimental studies of fatigue cracks. Eng Fract Mech 1991;39:113–30.
[13] Dougherty JD, Padovan J, Srivatsan TS. Fatigue crack propagation and closure behavior of modified 1070 steel: finite element study. Engineering Fracture Mechanics 1997;56:189–212.
[14] Gonzalez-Herrera A, Zapatero J. Influence of minimum element size to determine crack closure stress by the finite element method. Eng Fract Mech 2005;72:337–55.
[15] Antunes FV, Borrego LFP, Costa JD, Ferreira JM. A numerical study of fatigue crack closure induced by plasticity. Fatig Fract Eng Mater Struct 2004;27:825–35.
[16] Solanki K, Daniewicz SR, Newman Jr JC. Finite element modeling of plasticity-induced crack closure with emphasis on geometry and mesh refinement effects. Eng Fract Mech 2003;70:1475–89.
[17] Jiang Y, Feng M, Ding F. A reexamination of plasticity-induced crack closure in fatigue crack propagation. Int J Plast 2005;21:1720–40.
[18] Jiang Y, Sehitoglu H. Modeling of cyclic ratchetting plasticity, Part I: development of constitutive relations. ASME J Appl Mech 1996;63:720–5.
[19] Jiang Y, Sehitoglu H. Modeling of cyclic ratchetting plasticity, Part II: comparison with model simulations and experiments. ASME J Appl Mech 1996;63:726–33.
[20] Alizadeh H, Simandjuntak S, Smith D, Pavier M. Prediction of fatigue crack growth rates using crack closure finite element analysis. Int J Fatig 2007;29:1711–5.
[21] Antunes FV, Rodrigues DM. Numerical simulation of plasticity induced crack closure: identification and discussion of parameters. Eng Fract Mech 2008;75(10):3101–20.
[22] de Matos PFP, Nowell D. On the accurate assessment of crack opening and closing stresses in plasticity-induced fatigue crack closure problems. Eng Fract Mech 2007;74:1579–601.
[23] Pommier S, Bompard P. Bauschinger effect of alloys and plasticity-induced crack closure: a finite element study. Fatig Fract Eng Mater Struct 2000;23:129–39.
[24] de Matos PFP, Nowell D. Numerical simulation of plasticity-induced fatigue crack closure with emphasis on the crack growth scheme: 2d and 3d analyses. Eng Fract Mech 2008;75(8):2087–114.
[25] Zhao LG, Tong J, Byrne J. The evolution of the stress–strain fields near a fatigue crack tip and plasticity induced crack closure revisited. Fatig Fract Eng Mater Struct 2004;27:19–29.
[26] Pommier S. Plane strain crack closure and cyclic hardening. Eng Fract Mech 2002;69:25–44.
[27] McClung RC, Sehitoglu H. On the finite element analysis of fatigue crack closure – 1. Basic modeling issues. Eng Fract Mech 1989;33:237–52.
[28] Roychowdhury S, Dodds Jr RH. Effect of *T*-stress on fatigue crack closure in 3-d small-scale yielding. Int J Solids Struct 2004;41:2581–606.